Medium and Small Aperture Speckle Interferometry for Geostationary On-Orbit-Servicing Space Surveillance

Robert (Lauchie) Scott, PhD, P.Eng.
Defence R&D Canada Ottawa, 3701 Carling Avenue, Ottawa, ON, K1A 0Z4

Abstract

On-Orbit-Servicing (OOS) in Geostationary Equatorial Orbit (GEO) is likely to become a space mission reality provoking new problems for the optical space surveillance community. OOS' close-proximity flight of servicer and client satellites with separations less than 1 kilometer in GEO challenge the metric measurement capabilities of medium and small aperture space surveillance instruments. This paper describes an OOS monitoring technique based on Cross-Spectrum speckle interferometry to compensate for atmospheric turbulence and measure the OOS satellites' differential relative position. Cross-Spectrum speckle interferometry, an astronomical technique developed to measure the astrometric positions of binary stars, was adapted to the geostationary OOS problem and was tested using Sloan *i'* observations of co-located geostationary satellites. Medium (1.6m) and small (0.35m) aperture telescopes were used to observe these satellites undergoing optical conjunctions where their apparent line-of-sight separation narrowed within 5 arcseconds. During the initial development of the Cross-Spectrum approach some weaknesses were identified where particle strikes, faint background stars, anomalous fringe orientation angles and high relative angular rates corrupt the relative position measurement process. In this paper, newly adjusted compensation techniques to remedy these issues are described and the data is reprocessed. The Cross-Spectrum's performance is shown to work well on closely-spaced GEO satellites with separations less than 3 arcseconds and evidence is shown suggesting the technique can measure satellite separations within 1.8 arcseconds.

1. INTRODUCTION

On Orbit Servicing (OOS) is a new space mission profile that has been demonstrated in Low Earth Orbit [1] and is planned for near-term deployment into Geostationary (GEO) orbit [2]. The technologies being developed for OOS for GEO satellite servicing offer exciting new GEO mission options such as in-situ spacecraft inspection, robotic assistance to release of stuck solar arrays and antennas, replenishment and repair - such as battery replacement, hydrazine propellant refueling and technology refresh [2]. Orbital tug services removing derelict satellites from the GEO protected zone could help reduce conjunction hazards to operating satellites and mitigate the generation of space debris.

OOS in GEO poses new challenges to the optical space surveillance community due to the close-proximity between client and servicing satellites when viewed at long range. The satellite pair's proximity subtends angular distances smaller than the seeing disk of Earth's atmosphere blurring the satellite pair together into the same Point Spread Function (psf). Atmospheric turbulence limits the effectiveness of ground-based space surveillance sensors for OOS when the client and servicer pair begins proximity operations with separations less than 1 kilometer, subtending an angle of less than 5 arcseconds when viewed from the ground. Given the limited availability of large aperture, high-resolution telescopes equipped with adaptive optics for space surveillance - a simplified approach to tracking OOS using higher availability small and medium-class telescopes is of value.

This paper describes a small aperture OOS monitoring technique based on Cross-Spectrum speckle interferometry using differential angles measurements of the servicer with respect to the client satellite. This technique can be used to measure the relative motion of a servicing satellite about its client assuming non-forced (non-propulsive) motion in GEO. Speckle interferometry, an astronomical technique developed to measure relative astrometric positions of binary stars, was adapted to the geostationary OOS tracking problem. This technique was tested using medium (1.6m) and small (0.35m) aperture telescopes observing colocated GEO satellites passing near one another in 2014 and 2015 [3].

Some weaknesses of OOS Cross-Spectrum speckle interferometry have been identified and this paper describes techniques to mitigate them. These effects are due to the relative motion of stars in the detector field of view, the presence of cosmic ray hits on a high-speed detector, spurious fringe orientation angle measurements inferred during image processing and fringe rotation when the objects have close apparent separations. To begin, a quick description of Cross-Spectrum speckle interferometry is presented, basic instrument descriptions are provided and techniques to

mitigate these weaknesses are addressed. This paper concludes with reprocessed close-approaches between GEO satellites to test this technique's effectiveness and its performance indicated.

2. OOS OBSERVATION CASES COMPARED TO TYPICAL SPACE SURVEILLANCE TRACKING

Ground-based OOS tracking using speckle interferometry is a specialized observing case compared to typical CCD based satellite tracking. Ground-based OOS observing considers geosynchronous satellites in formation flight with in-track and cross-track separations less than 1 kilometer from one another subtending an angular equivalent less than 5 arcseconds viewed at geostationary ranges (Fig.1). This 1-km (~5-arcsecond) inter-satellite distance is the upper limit for OOS speckle observations in the plane of the sky. When viewed through Earth's atmosphere, this 5-arcsecond limit is consistent with the size of the isoplanatic patch ($\Delta\theta_{iso}$), the characteristic size of atmospheric turbulence cells that coherently refract light [4]. Speckles imaged within this patch would appear to have correlated, duplicating speckle patterns (Fig. 2 left). Separations larger than 5 arcseconds are more likely to refract light across different turbulence cells causing speckles to decorrelate during imaging (Fig. 2 right).

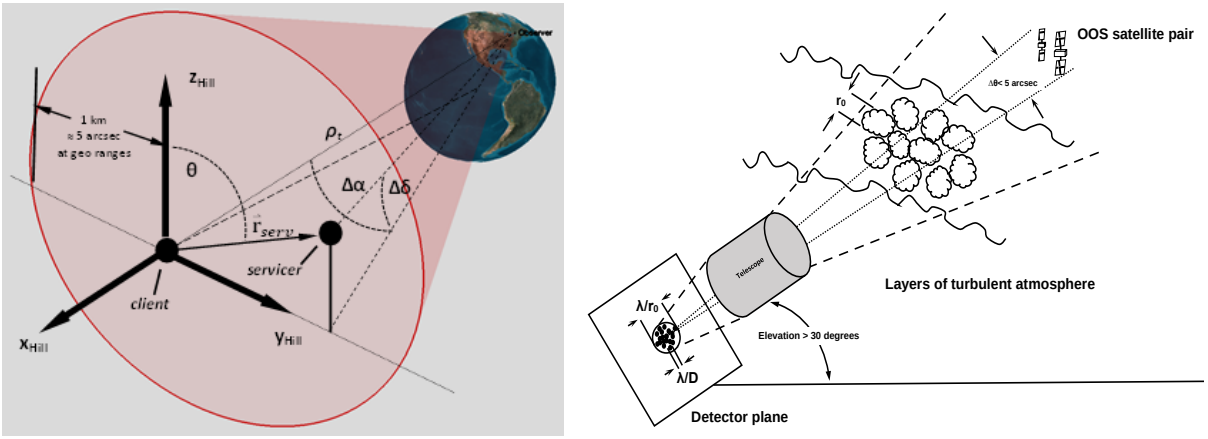

Fig.1 (***Left***): Formation geometry of OOS client and servicer satellites, the Hill coordinate frame centered on the client and definition of differential angles $\Delta\alpha$, $\Delta\delta$. Both objects are presumed to be within one kilometer (5 arcseconds) the plane of the sky. (***Right***): Viewing geometry of closely-spaced astronomical through the Earth's atmosphere within the isoplanatic patch.

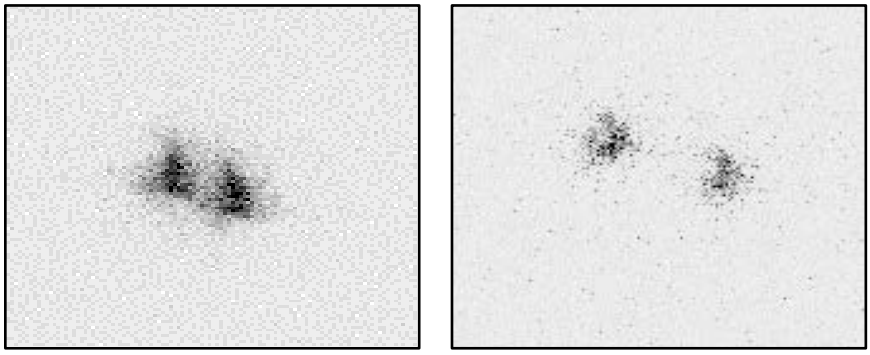

Fig.2 (***Left***): Binary star pair STF2644 with separation of 2.7 arcseconds exhibiting coherence of speckles. (***Right***): BAL1202 with a separation of 8.4 arcseconds showing different speckle patterns.

3. CROSS-SPECTRUM SPECKLE INTERFEROMETRY

Speckle interferometry has been used to measure closely-spaced binary stars since its introduction by Labeyrie in 1970 [5]. This process stacks the Fourier transform of hundreds to thousands of short-exposure (~10 msec) speckle images to freeze the turbulence profile of the atmosphere. These speckle images are Fourier transformed and a stacked creating a combined power spectrum (Fig. 3b). Analysis of the fringe pattern can determine the separation distance ρ and orientation angle θ_{fringe} between two closely-spaced astronomical objects approaching the diffraction limit of the telescope. Note that the fringe direction is perpendicular to the true orientation direction to the secondary object.

While Labeyrie Speckle Interferometry is computationally and conceptually simple, the symmetry of the Fourier transform creates a 180-degree ambiguity in the direction to the secondary object (Fig. 3c) relative to the primary (usually the brighter object). This positional ambiguity is of limited use in practical space surveillance applications. To overcome this issue, Cross-Spectrum speckle interferometry, as described by Aristidi et al. [6], can be used to preserve the resolution capabilities of speckle interferometry while uniquely identifying the true direction of the secondary object. Cross-Spectrum speckle interferometry collects the same short-exposure imagery and stacks their transformed speckle images similar to Labeyrie's technique, but squares the intensity of the pixel values multiplied by the complex conjugate of the Fourier transform of the image itself (Fig 3d-3f). Analysis of the Cross-Spectrum fringes (Fig 3e) enables relative position measurement of the two closely-spaced objects by measuring fringe orientation angle, the fringe separation distances and the true direction toward the secondary object by analysis of the fringe gradient at the center of the Cross-Spectrum.

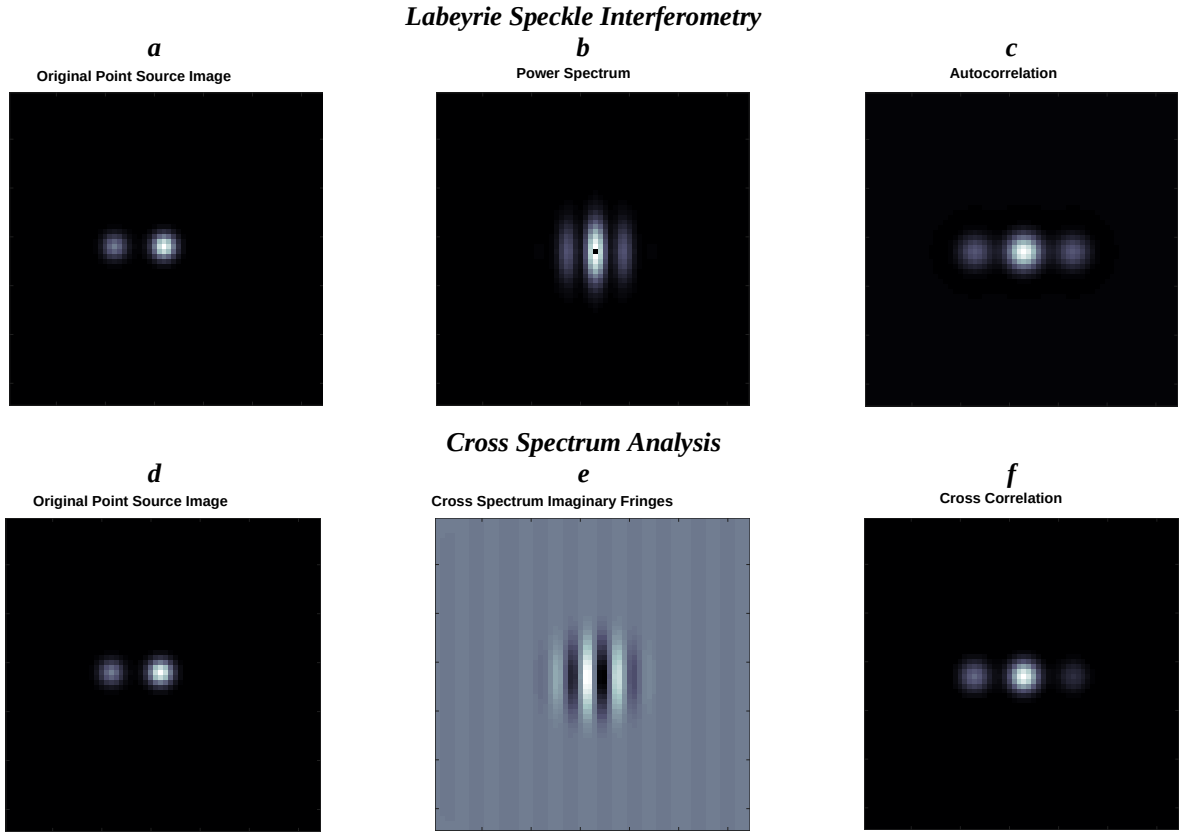

Fig.3 (***Top row***): Labeyrie Speckle Interferometry. (***Bottom row***): Cross-Spectrum. Note the fringes of the Cross-Spectrum are biased in the direction of the secondary object compared to the Labeyrie Speckle Interferometry's power spectrum

The Cross-Spectrum is computed by using the *zero-mean image* $\hat{I}(x)$ and *zero-mean speckle* $\hat{S}(x)$ of the optical system's point spread function

$$\hat{I}(x) = I(x) - \bar{I} \quad \text{and} \quad \hat{S}(x) = S(x) - \bar{S} \tag{1} \tag{2}$$

where $\bar{I}$ and $\bar{S}$ are the arithmetic means of a short-exposure speckle image $I(x)$ and the point source function $S(x)$. The Fourier transform $\mathcal{F}$ acting on $\hat{I}^2(x)$ and the complex conjugate $\mathcal{F}(\hat{I})$ captures the image spatial frequency information as

$$\widehat{K}_{\hat{I}}(u) = \langle \mathcal{F}(\hat{I}^2) \cdot \mathcal{F}(\hat{I})^* \rangle \tag{3}$$

where the $\langle\ \rangle$ notation denotes the ensemble average. This permits the following approximations [6] to simplify the employment of the Cross-Spectrum[1] where

$$K_{\hat{I}}(\rho) = K_{\hat{S}}(\rho) * K_O(\rho) \tag{4}$$

$$K_I(u) = \widehat{K}_{\hat{S}}(u) \cdot \widehat{K}_O(u) \tag{5}$$

where ρ is the separation distance between the objects in the spatial plane and u denotes spatial frequency in cycles per frame and * denotes the convolution between the point spread function $K_{\hat{S}}(\rho)$ and the object function $K_O(\rho)$.

All the information needed to describe the relative position between two closely-spaced astronomical objects can be found by inspecting the properties of the imaginary component of the Cross-Spectrum's $K_{\hat{I}}(u)$ fringes. These fringes are modulated by the spatial representation of the psf $\widehat{K}_{\hat{S}}(u)$ and a set of sinusoidal fringes with a spatial frequency of d such that

$$Im(\widehat{K}_{\hat{I}}(u)) = \widehat{K}_{\hat{S}}(u)[\alpha_b(1 - \alpha_b)\, sin(2\pi u d)] \tag{6}$$

where d is the separation between the objects[2] and α_b is the ratio of brightness of servicer to the client satellite (by definition $\alpha_b < 1$). Defining $\alpha_b < 1$ posits that the slope of the fringes at the center of the Cross-Spectrum has a positive gradient in the direction of the secondary object.

Differential right ascension $\Delta\alpha$ and differential declination $\Delta\delta$ can be formed by relating the polar coordinates (ρ,θ) which are commonly used by the binary star community by expressing

$$\begin{bmatrix} \Delta\alpha \\ \Delta\delta \end{bmatrix} = \rho \begin{bmatrix} \sin(\theta) \\ \cos(\theta) \end{bmatrix} \tag{7}$$

where ρ is the angular separation distance between the two objects in the plane of the detector. This forms the basis of relative motion estimates. These measurements require that the North direction on the detector must be known. The polar angle θ is measured eastward from celestial North (counterclockwise). Calibration of the θ angle relative to celestial North direction using the star trails technique is described in [3].

4. CONVERSION BETWEEN RELATIVE MOTION AND DIFFERENTIAL ANGLES

Space surveillance observations are normally used to compute satellite orbits in the Earth centered inertial reference frame. Closely-spaced objects in GEO have near-circular orbits where their relative motion is well described by the Clohessy Wiltshire, or Hill's equations (see Annex A). This relative motion model requires the measurement of *differential angles* $\Delta\alpha$, $\Delta\delta$ between the client and servicing satellite rather than measurement of *absolute angles* (α,δ) in order to describe the servicer's trajectory when using ground based measurements of its relative motion.;
It can be assumed that the observed topocentric declination δ_t of both client (the primary object) and servicer (secondary) is constant as the declination rate for GEO satellites is small. For many closely-spaced GEO satellites, the

[1] This approximation requires that the distance between the objects must be larger than the size of the speckle [6].

[2] Conversion between the spatial frequency between two objects in an image to the spatial separation can be performed by using the relationship $d = Na_p/F_s$ where d is the separation distance in arcseconds, a_p is the pixel pitch of the detector in arcseconds/pixel, F_s is the fringe separation distance in cycles/frame and N is the size of the frame in pixels/frame.

hour-angle difference between geocentric right ascension and topocentric right ascension $(\alpha - \alpha_t)$ can also be assumed to be constant. The topocentric range ρ_t from the observer to the satellites can also be assumed to be constant. This creates a simplified relationship describing the relative motion of the servicing satellite with respect to the client [3] where

$$\begin{bmatrix}\Delta\alpha \\ \Delta\delta\end{bmatrix} = \frac{1}{\rho_t}\begin{bmatrix}\frac{\sin(\alpha-\alpha_t)}{\cos(\delta_t)} & \frac{\cos(\alpha-\alpha_t)}{\cos(\delta_t)} & 0 \\ -\cos(\alpha-\alpha_t)\sin(\delta_t) & sin(\alpha-\alpha_t)\sin(\delta_t) & \cos(\delta_t)\end{bmatrix}\begin{bmatrix}x \\ y \\ z\end{bmatrix}_{Hill} \quad \text{where} \quad \mathbf{x} = \begin{bmatrix}x \\ y \\ z\end{bmatrix}_{Hill} \qquad (8),(9)$$

Measurements of the relative position of the servicer relative to the client can be made using equation 7. Equation 8 relates the differential angles measurements $[\Delta\alpha\ \Delta\delta]^T$ to the state vector $\mathbf{x}$ of the servicer in the Hill frame centered on the client. A linearized Kalman filter be formed using Hill's equations[3] as a dynamic model to estimate the relative position and velocity of the servicer. This information can be used to describe the type of motion a servicer is performing about a client; such as a simply flyby or if the servicer is on an intercept trajectory with the client.

5. INSTRUMENTATION

It is essential that at least two detector pixels sample the Airy radius of the instrument's psf to properly sample a speckle. For the measurements collected in the experiments performed in 2014 and 2015, this required various combinations of 2x and 4x barlow lenses to project the speckles onto the detector. An estimate of the psf radius is

$$psf = 1.22\lambda f\# \qquad (10)$$

where λ is the wavelength of detection and $f\#$ is the ratio of the telescope focal length to aperture diameter. Longer focal ratio instruments of *f/10* or more are preferred for speckle interferometry as it is easier to sample the speckles with modest focal length extension. The detector technology used to image the speckles were 1024x1024 Electron Multiplying CCDs (EMCCDs). These detectors can rapidly acquire (>10 Hz) short exposure (~10 millisecond) imagery of object speckles making them well-suited for this application. Chromatic dispersion [9] is mitigated by passing light through a Sloan *i'* photometric filter reducing elevation effects when detecting speckles.

The telescopes used in these tests were the 1.6m Mont Megantic telescope [7] and the 0.35m DRDC Ottawa Space Surveillance telescope [8] (Fig 4). Both instruments were fitted with the filters, EMCCDs and barlow lens arrangements in order to properly sample the speckles from each instrument.

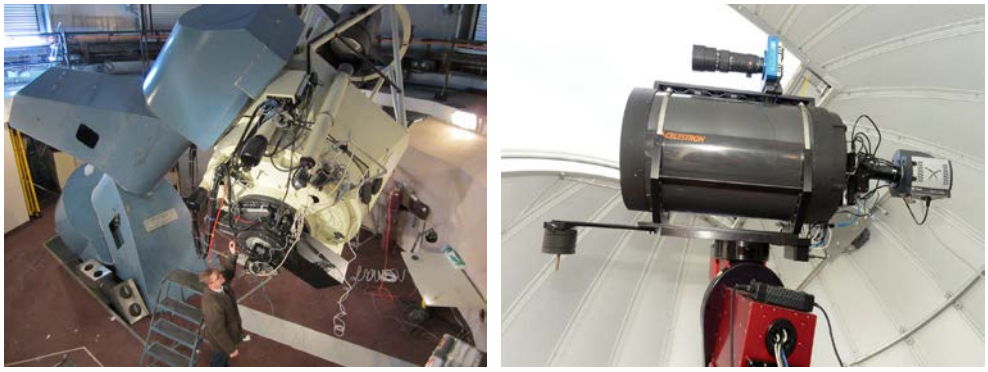

Fig.4 (***Left***): Medium-aperture Mont Mégantic 1.6m telescope (***Right***) Small-aperture DRDC Ottawa 0.35m Space Surveillance Observatory. Image Credits Ref. [3], Janice Lang, DRDC Ottawa

6. SPECKLE INTERFEROMETRY OBSERVATIONS OF GEO SATELLITES

[3] Optionally differential Solar Radiation Pressure (dSRP) modelling can also be incorporated [10]. SRP modelling is recommended for observation intervals of 6 hours or more.

Optical conjunctions [11] of geostationary satellites were used to test this technique on actual moving satellites. Optical conjunctions are occasional events where two co-located GEO satellites *appear* to conjunct with one another with respect to an observer's line-of-sight. There is little risk of actual collision between satellites as they are separated by more than 10 km radially during their station-keeping operations. While actual OOS missions are in much closer proximity to one another and move at much slower relative angular rates, these optical conjunctions provide short-duration test cases for Cross-Spectrum speckle interferometry as actual OOS missions are yet to be flown. Binary stars are also useful, but do not exhibit the relative motion aspects provoking practical issues in image processing (see section 7a). Three test cases are re-examined in this paper corresponding to the medium and small-aperture class telescope observations of GEO satellites. Optical conjunctions between Anik G1, Anik F1R and Anik F1, Anik G1 were observed using the 1.6m Mont Mégantic telescope in February 2014. One optical conjunction of Anik F1, Anik G1 was observed using the 0.35m DRDC Ottawa Space Surveillance Research Telescope in August 2015. Sample imagery showing the speckled images of these satellites is shown in Fig. 5.

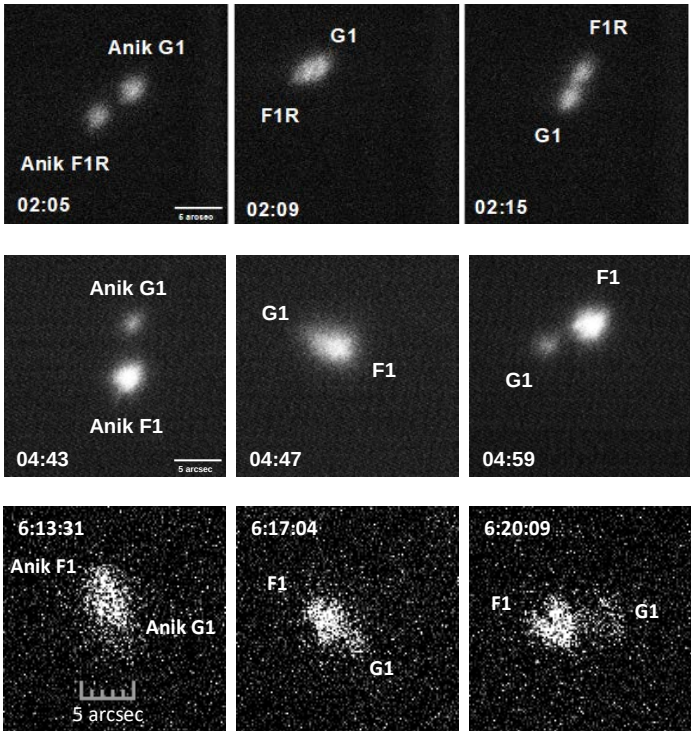

Fig.5 (***Top row***): Mont Mégantic 1.6m observations of the optical conjunction between 18 Feb 2014 - Anik G1, Anik F1R (***Middle row***): Mont Mégantic 1.6m observations of Anik F1, Anik G1. (***Bottom row***): DRDC Ottawa Space Surveillance Observatory 0.35m images of Anik F1, Anik G1. Image credit: Ref. [3].

7. MODIFICATIONS TO CROSS SPECTRUM SPECKLE INTERFEROMETRY UNIQUE TO SPACE SURVEILLANCE OBSERVATIONS

Applying Cross-Spectrum speckle interferometry to the space surveillance of closely-spaced objects requires some special image processing considerations. The moving nature of the geosynchronous satellites and the fast acquisition mode of the detector forces image processing considerations not usually performed in wide-field space surveillance tracking. Three of these considerations are described as follows:

7a. Cosmic Ray and Background Star Removal

A common blemish occurring in many astronomical CCDs is high energy particle strikes from cosmic rays. These cosmic ray hits appear as strong intensity spikes and are generally ignored during regular ground-based space surveillance processing. During speckle imaging, these cosmic ray hits can corrupt the fringe formation process as they contain comparable aggregate pixel intensity as the entire speckled satellite pair. This causes out-of-character fringes corrupting the Cross-Spectrum stacks (Fig. 6 center).

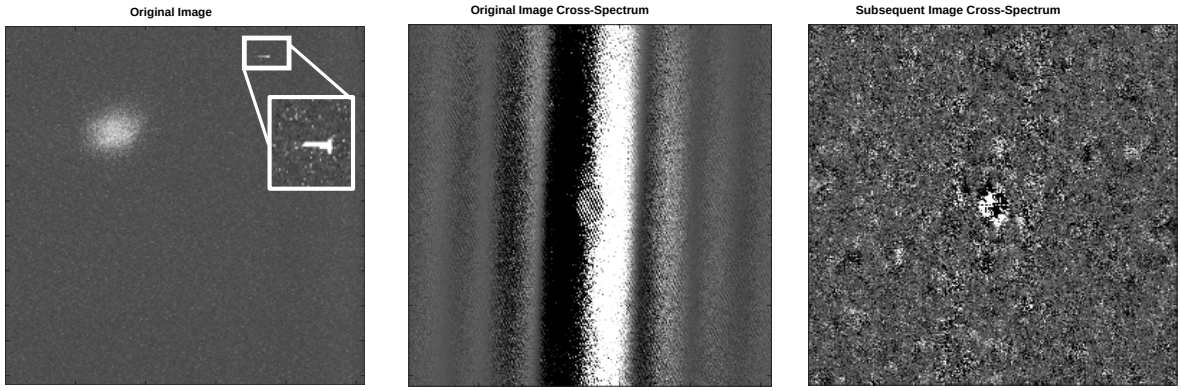

Fig.6 (***Left***): Cosmic Ray strike on EMCCD Image (inset). (***Center***): Cross Spectrum of image containing cosmic ray strike. (***Right***): Subsequent frame's Cross-Spectrum showing drastically different fringes as no cosmic ray strikes were encountered.

A further complication is that geosynchronous satellites move relative to the background stars during speckle imaging. Occasionally these stars appear in the detector field of view (see Fig.7) provoking additional fringes with frame-to-frame variation in their fringe separation and orientation. This corrupts the fringe stacking for the two closely-spaced satellite objects.

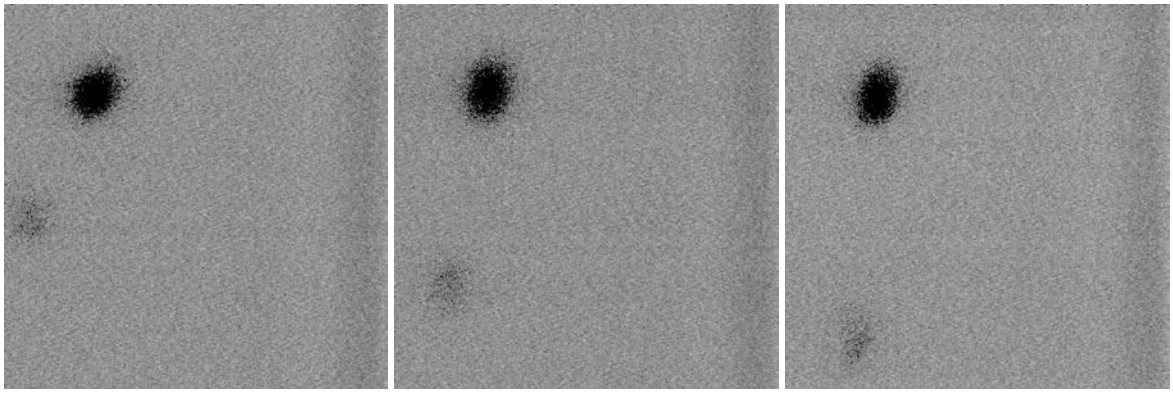

Fig.7 Sequence of frames where Anik G1, Anik F1R are tightly clustered (upper left), and a faint star traverses the field of view (lower left).

An efficient way to reject speckle images containing either cosmic rays or star blemishes is to monitor the speckle image backgrounds' standard deviation σ by forming a moving average of these σ values. Images containing either of these blemishes can be rejected by checking if they breach the moving average's trend level by more than three times that variation in the moving average itself. Images where the background jumps by more than 3σ is generally a reliable indicator of the presence of a passing star. Larger jumps of 10σ or more is usually an indicator of a cosmic ray hit (see Fig. 8). If the 3σ limit line is breached, the image is rejected from the stacking process and the subsequent image is processed.

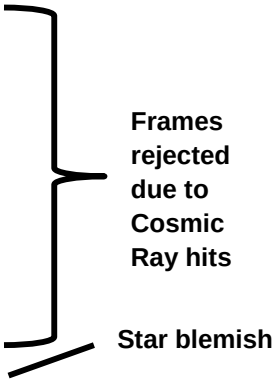

Fig.8 Speckle frames rejected due to image background standard deviations exceeding the moving average limit (blue dashed line)

7b. Fringe Orientation Angle Measurement

The fringe orientation angle θ_{fringe} is the first step performed to determine the separation between the client and servicing satellite. The Radon transform automatically detects linear features in an image by projecting the sum of pixel values at various angular orientations about it and was used in the first implementation of the image processing software. The integrated pixel intensity peak produced by these angular projections is an indicator of the dominant linear feature in an image. Occasionally, when analyzing broader fringes, the Radon transform tends to favor diagonals across the width of a fringe (Fig. 9) corrupting the fringe orientation angle measurements. This effect was observed in the initial analyses of the Mont Mégantic and DRDC Space Surveillance telescope satellite speckle data [3]. A remedy for this effect is to use a Sobel filter to expose fringe edge features, thinning the width of the input into the Radon transform making fringe orientation angle measurements more reliable [3].

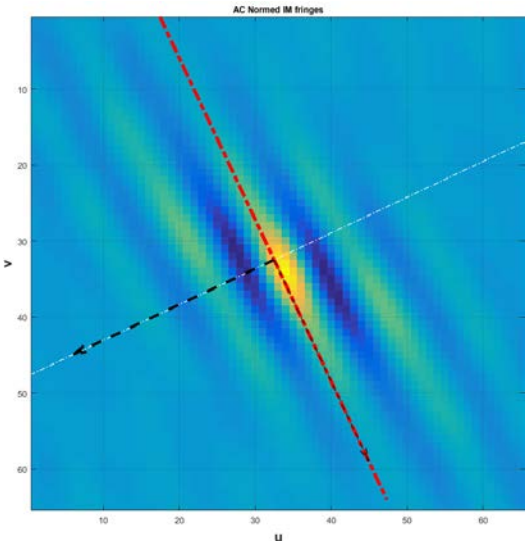

Fig.9. Radon transform detection of the orientation angle of the fringes. Note the slight misalignment of the detected orientation angle (red dashed line) compared to the fringe direction.

An improvement in the measurement of fringe orientation angles was made in this reanalysis of the 2014 and 2015 data by applying a Hough transform to the Sobel filtered images. In contrast to the singular orientation angle returned by the Radon transform, the Hough transform extracts *multiple* line segments for each detected linear feature in an image. As parallel fringes have similar orientation angles, a simple average of the Hough transform's θ_{fringe} results provide a more consistent measurement of the fringe orientation angles.

7c. Fringe smearing due to fringe rotation rate

A final correction handles a rarer, more extreme case of relative motion between a client and servicing satellite. In some circumstances, high apparent rotational angular rates of the servicer about the primary can be observed. This occurs when the apparent radial separation ρ between objects is small and there is observable relative motion ω_0 between them (Fig. 10). This provokes the Cross-Spectrum fringes to rotationally smear during the stacking process. OOS formation flight in GEO is less likely to provoke this type of behavior however this correction may be needed if the apparent separation between the OOS satellites is small, and relative motion between the fringes is observable.

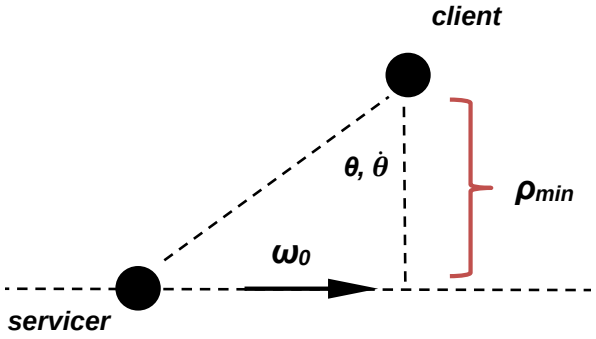

$$\dot{\theta} = \frac{-\left(\rho_{min}/\omega_0\right)}{\left(\rho_{min}/\omega_0\right)^2 + (t - t_0)^2} \tag{11}$$

Fig.10: Motion of servicing satellite with respect to the client spacecraft

When the angular rates of the fringes are the highest, the fringe separation distance can be assumed to be constant. Frames exceeding ½ pixel of rotation at the edges of the image the speckle images can be rotationally transformed by $-\Delta\theta$ to remove the smearing effect. This de-rotation approach is implemented by coupling the relative orbit estimation to the image processing of the speckle images. The relative orbit state estimate $\mathbf{x} = [x \quad y \quad z]^{\boldsymbol{T}}_{\boldsymbol{Hill}}$ can be used to estimate of amount of fringe rotation on each speckle image.

The Hill coordinates describing the position of the servicer relative to the client must be transformed into the sensor-frame coordinates by creating forming the rotation matrix

$$\mathbf{R}^{Hill}_{cam} = \frac{1}{\rho_t}[\mathbf{R}_2(-\delta_t)\mathbf{R}_3(-(\alpha - \alpha_t))] \tag{12}$$

where $\mathbf{R}_2$ and $\mathbf{R}_3$ are Euler rotations. The $\mathbf{R}^{Hill}_{cam}$ rotation matrix can then be used to form camera frame coordinates by transforming the Hill frame position and velocity vector of the servicing satellite

$$\begin{bmatrix}\vec{\boldsymbol{r}}_{\boldsymbol{cam}} \\ \vec{\boldsymbol{v}}_{\boldsymbol{cam}}\end{bmatrix} = \mathbf{R}^{Hill}_{cam}\begin{bmatrix}\mathbf{I}_{3x3} & \mathbf{0}_{3x3} \\ \mathbf{0}_{3x3} & \mathbf{I}_{3x3}\end{bmatrix}\begin{bmatrix}\vec{\boldsymbol{r}}_{\boldsymbol{Hill}} \\ \vec{\boldsymbol{v}}_{\boldsymbol{Hill}}\end{bmatrix} \qquad \mathbf{I}_{3x3} = \begin{bmatrix}1 & 0 & 0 \\ 0 & 1 & 0 \\ 0 & 0 & 1\end{bmatrix} \tag{13}$$

Equations 14 and 15 provide the final transformation from camera to image coordinates. Radial coordinate information is meaningless in a 2-dimensional camera image therefore its scalar value is discarded (*null).* The camera's image coordinates x_{image}, y_{image} can be extracted to form the basis of the projection of the OOS satellites onto an image. The y_{cam} direction is flipped as the x_{image} coordinates are positive in a direction opposite to the eastward convention used for Hill's coordinates. Similarly, most images use the camera y-axis convention (y_{image}) being positive downward, necessitating the sign flip of z_{cam}.

$$\begin{bmatrix} Null \\ \vec{\mathbf{r}}_{image} \end{bmatrix} = \begin{bmatrix} Null \\ \begin{bmatrix} x_{image} \\ y_{image} \end{bmatrix} \end{bmatrix} = \begin{bmatrix} x_{cam} \\ -y_{cam} \\ -z_{cam} \end{bmatrix} \qquad \begin{bmatrix} Null \\ \vec{\mathbf{v}}_{image} \end{bmatrix} = \begin{bmatrix} Null \\ \begin{bmatrix} \dot{x}_{image} \\ \dot{y}_{image} \end{bmatrix} \end{bmatrix} = \begin{bmatrix} \dot{x}_{cam} \\ -\dot{y}_{cam} \\ -\dot{z}_{cam} \end{bmatrix} \quad (14)\ (15)$$

Using these measurements the rate of rotation of the fringes can be estimated by equation 16.

$$\dot{\theta} = \left| \frac{1}{\rho} \left(\vec{\mathbf{r}}_{image} \times \vec{\mathbf{v}}_{image} \right) \right| \quad (16)$$

A single-step estimate of the amount of de-rotation $\Delta\theta$ needed for each frame is found by using the equation 16 and the time of the selected j^{th} image with respect to the time of the start of each stack.

$$\Delta\theta = -\dot{\theta}\, \Delta t_j^{stack} \quad (17)$$

8. MODIFIED CROSS-SPECTRUM TRACK PERFORMANCE RESULTS

The 2014 and 2015 speckle images of GEO satellite optical conjunctions were reprocessed and the relative position of the secondary (servicing) satellite relative to its primary (client) satellite was measured. A summary of the tracking data is shown in Table 1 detailing the satellite identifies, sensors used to collect the speckle images and the measured minimum separation and object brightnesses. The measured tracks of the secondary with respect to the primary are shown in Fig 11 and their starting location and directions of motion are indicated by arrows. The minimum approach distance, for each track was estimated using a quadratic least squares fit using the same technique as described by Knox in [12].

Table 1: Track Summary

Track	Primary	Secondary	Sensor	Start of Track Date (UTC)	ρ_{min} (arcsec)	$\mathbf{m}_{primary}$	Δm (α_b)
1	Anik G1	Anik F1R	Med. 1.6m	18 Feb 2014 02:05	1.85 ± 0.30	10.2	0.36 (0.72)
2	Anik F1	Anik G1	Med. 1.6m	18 Feb 2014 04:03	3.34 ± 0.08	9.03	1.53 (0.24)
3	Anik F1	AnikG1	Small 0.35m	02 Aug 2015 06:13	3.10 ± 0.07	9.67	1.63 (0.22)

Some features are immediately noticeable upon inspection of the tracks in Fig 11. The medium aperture sensor shows better positioning uncertainty on Tracks 1 and 2 compared to Track 3 which was measured using the small aperture sensor. This is attributable to the larger psf of the small telescope (0.52 arcseconds compared to 0.11 arcseconds for the medium aperture sensor).

Also visible in Figure 11 are breaks in tracking data for both Track 1 and Track 3. This is due to mount tracking issues on the satellite pairs. As geostationary satellites have very small declination rates from a ground observer's perspective, the break in Track 1 is due to both satellite objects drifting toward the top of the field of view during imaging. To re-center the satellites, a re-slew of the mount was required and the pair was re-centered in the field of view of the detector. This caused a momentary interruption in imaging. The break in Track 3 was due to the telescope mount unexpectedly ceasing tracking on the satellite pair and a similar re-centering process was performed.

Figs. 12 through Fig. 14 decomposes each track into constituent ρ,θ measurements of the Cross-Spectrum's fringe shape. In Fig. 12, Track 1 shows better orientation angle consistency compared to the old processing. This is attributed to the improved orientation angle measurements from the Hough transform. Tracks 2 and 3 have closest approaches of ~3 arcseconds but show tracking performance similar to the original image processing algorithm. The improvements tended to work best on Track 1 where the two objects had their closest approach to one another.

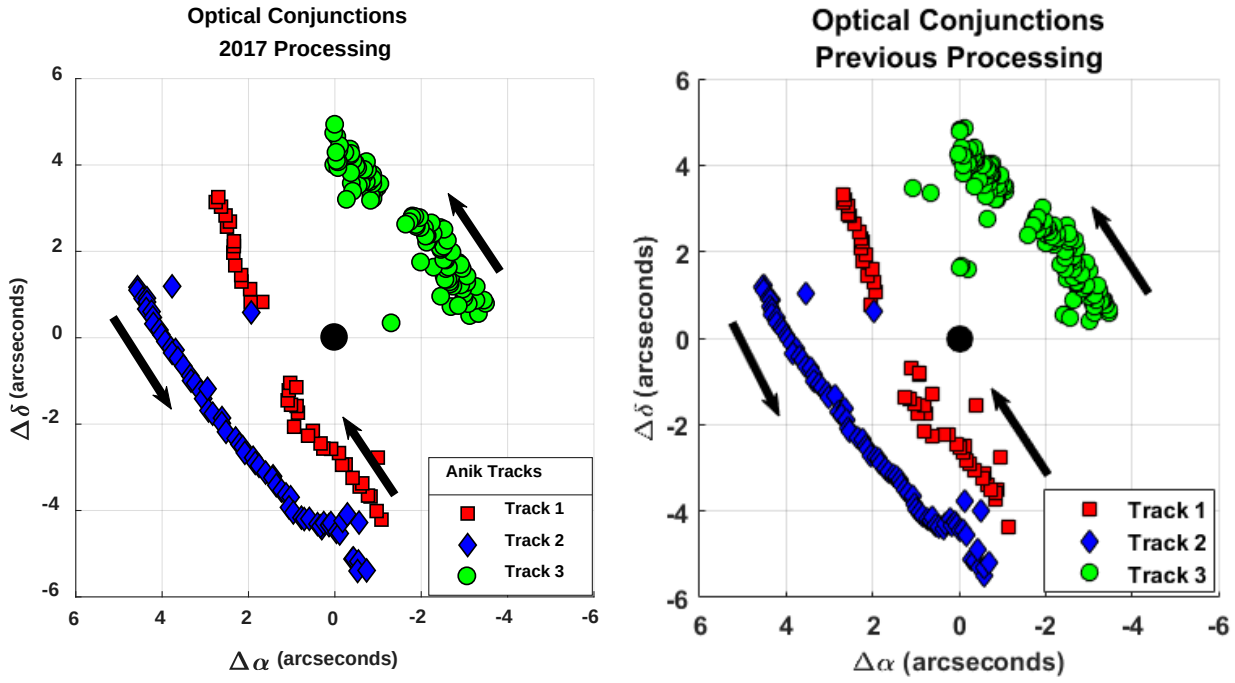

Fig.11: ***(Left):*** New processing of the satellite passes ***(Right):*** Old processing approach. Note the reversed Δα direction to coincide with the observed Eastward direction of motion.

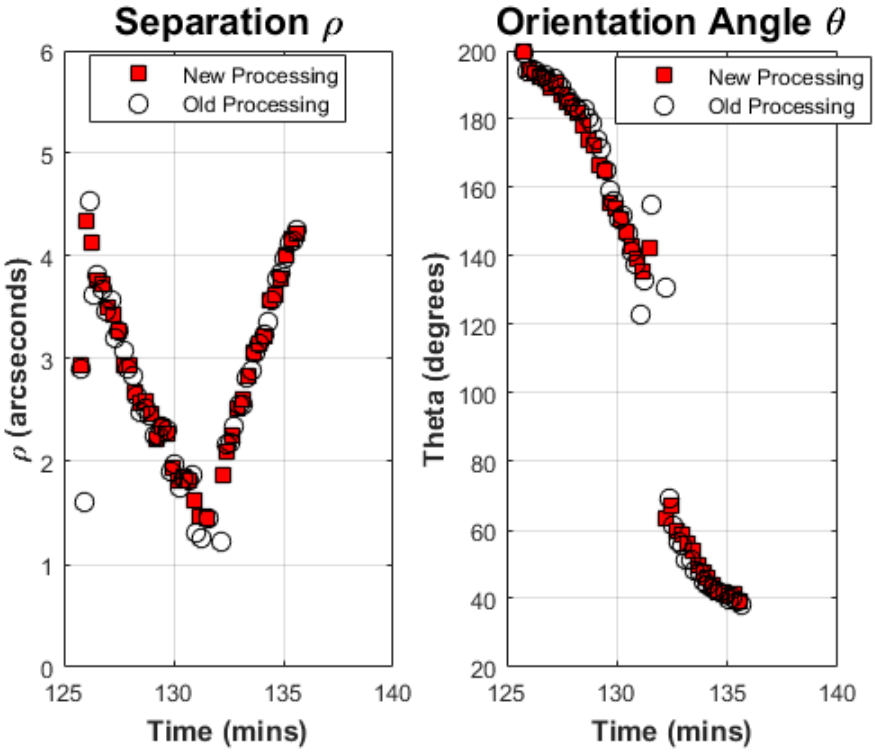

Fig.12: Track 1: Anil G1, Anik F1R separation distance ρ and Orientation Angle θ results

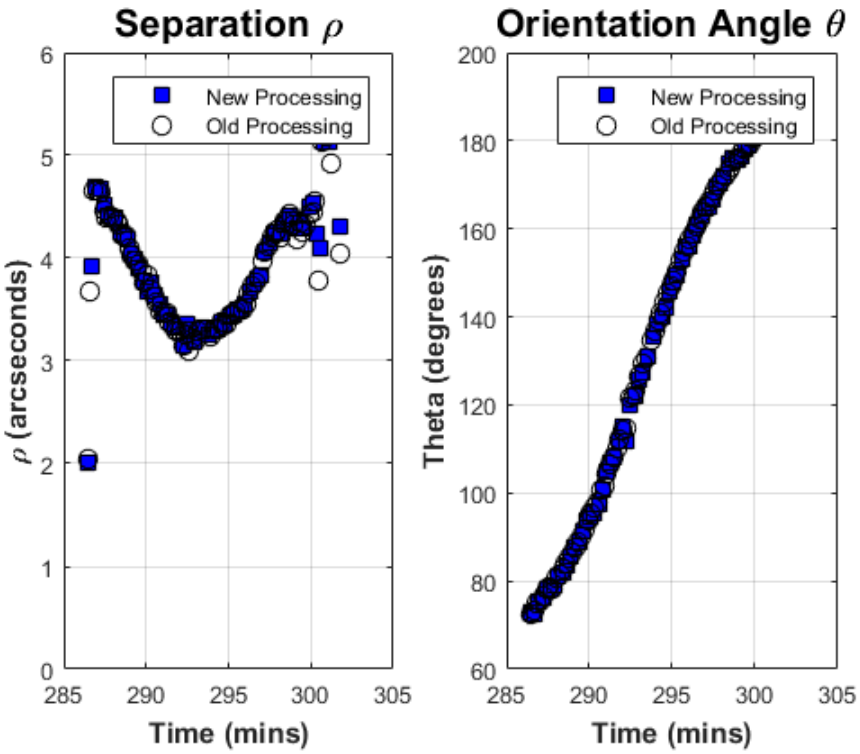

Fig.13: Track 2: Anik F1, Anik G1 separation distance ρ and Orientation Angle θ results

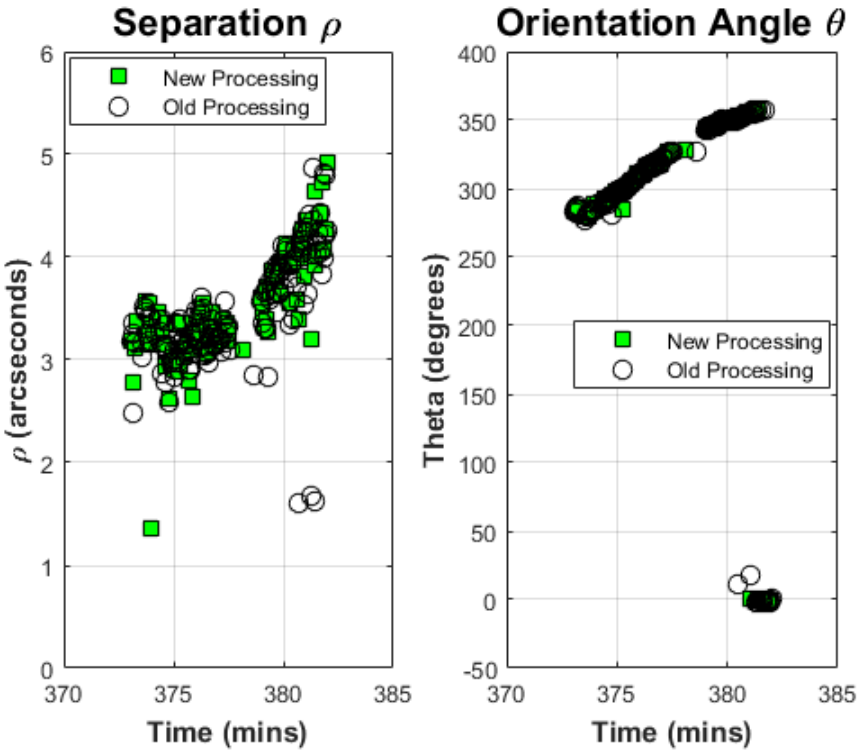

Fig.14: Track 3: Anik F1, Anik G1 separation distance ρ and Orientation Angle θ results

In all tracks when the separation distance ρ between the satellites exceeded 4.5 arcseconds, spurious ρ measurements were obtained. This is visible at the start and finish of all tracks in Figs. 12 through 14. This is likely due to the satellites' separation spanning two different turbulence cells outside of the isoplanatic limit reducing the effectiveness of the Cross-Spectrum process. The upper limit of 5 arcseconds is likely best applied for cases when seeing conditions are very steady. Generally, the Cross-Spectrum approach is likely best applied when intersatellite separations are less than 4 arcseconds when viewed under moderate seeing conditions. The seeing conditions measured during the 2014 and 2015 satellite observations varied between 2-3.5 arcseconds [3].

Both medium and small aperture telescopes performed well using the Cross-Spectrum technique to measure the relative position of Anik satellites passing within 4 arcseconds of each another in GEO. The medium aperture sensor recorded the closest approach where Anik G1 and Anik F1R (Track 1) closed within 1.8 arcseconds of one another. The Mont Megantic sensor tended to have best measurement precision of ~0.08 arcseconds in $\Delta\alpha$, $\Delta\delta$. In contrast, the small aperture sensor tended to have measurement precision of ~0.3 arcseconds per axis and is likely due to the broader psf of the instrument. Both instruments offer relatively good tracking accuracy for closely-spaced objects in GEO orbit however some improvement could be made with the small aperture system, such as shortening the exposures to increase the higher spatial frequency speckle content.

The Cross-Spectrum approach shows promise to observe OOS objects in GEO for objects within 5 arcseconds of one another. The improvements in the image processing described in this paper tended to largely correct images cases where spurious fringe orientation angles were measured. The improved image processing also tended to reject more images containing blemishes from cosmic ray hits. The fringe orientation angle smearing effect tended to have less of an impact in this reanalysis and is likely less of a concern in real GEO OOS cases. More test cases are recommended on moving satellites where the objects pass within 2 arcseconds of one another to fully validate that the fringe smearing effect is mitigated.

9. SUMMARY

Cross-Spectrum speckle interferometry was tested on optical conjunctions of colocated GEO satellites as a proof of concept to determine if this technique could be used to track closely-spaced objects performing OOS in GEO. This technique is limited to cases when the client and servicing satellite are within 5 arcseconds of one another when viewed from the ground. Improved cosmic ray and star blemish removal techniques and improved fringe orientation angle measurements were implemented in the Cross-Spectrum image processing software. These changes showed better performance compared to the original processing of this data. Satellites were measured to within 1.8 arcseconds of one another and differential angles measurement accuracies of 0.08 and 0.3 arcseconds for medium and small aperture sensors was obtained. Further testing is recommended for objects with separations less than 2 arcseconds to more fully validate this technique. When the first OOS satellites begin exciting new servicing missions in GEO orbit, medium and small aperture optical space surveillance sensors have a new tool to help monitor and track their activities.

10. REFERENCES

1 Mulder, T., "Orbital Express Autonomous Rendezvous and Capture Flight Operations, part 1 of 2: Mission Description, AR&C Exercises 1,2,3,", AAS Spaceflight Mechanics Meeting, 2008, Galveston TX, 2008.Space Based Space Surveillance System (SBSS), http://www.boeing.com/boeing/defense-space/space/satellite/sbss.page. Boeing Corporation, retrieved July 2013.

2 DARPA Robotic Servicing in Geostationary Orbit System (RSGS), https://www.darpa.mil/program/robotic-servicing-of-geosynchronous-satellites, retrieved 13 August 2017.

3 Scott, R.," A Method for Optical Tracking of on-Orbit Servicing Operations in Geostationary Orbit using Speckle Interferometry" PhD Dissertation, Carleton University, Ottawa, Canada, 2015.

4 Roddier, F., Gilli J.M., Vernin, J., "On the Isoplanatic Patch Size In Stellar Speckle Interferometry", J. Optics, Vol. 13 No.2, pp 63-70, 1982.

5 Labeyrie, A., "Attainment of Diffraction Limited Resolution in Large Telescopes by Fourier Analyzing Speckle Patterns in Star Images", Astronomy and Astrophysics, vol. 6, pp. 85-87, 1970.

6 Aristidi, E., Carbillet, M., Lyon, J-F, and Aime, C.," Imaging binary stars by the cross-correlation technique", Astronomy and Astrophysics Supplement series, vol. 125 (1997) 139-148.

7 Observatoire Mont Megantic, URL: http://www.omm.craq-astro.ca.

8 Wallace, B., Scott, R., Spaans, A., “The DRDC Ottawa Space Surveillance Observatory” Proceedings of the AMOS Technical Conference 2007, Maui Economic Development Board, Maui, HI, 2007.
9 Mason, B., "Atmospheric Dispersion and Risley Prisms", United States Naval Observatory, Double Star Report, No.3, 27 Jan 2003.
10 Kawase, S., “Real Time Relative Motion Monitoring For Co-located Geostationary satellites”, Journal of the Communications Research Laboratory, Tokyo, Japan Vol. 36, No 148, 1989.
11 Scott, R and Ellery, A., "Speckle Interferometry Tracking of On-Orbit Servicing in Geostationary Orbit", Journal of Spacecraft and Rockets, Vol. 53, No. 3 (2016), pp. 433-447, https://doi.org/10.2514/1.A33406.
12 Knox, K., “Measuring Close Binary Stars with Speckle Interferometry”, Proceedings of the AMOS Technical Conference, Maui HI., 2014.
13 Clohessy, W.H., Wiltshire, R.S., “Terminal Guidance system for satellite rendezvous”, Journal of Aerospace Sciences, Vol. 27, No. 9, 653-658, 674., 1960.
14 Hill, G., “Researches in Lunar Theory”, American Journal of Mathematics, 1, 5-26, 1878.
15 Vallado, D.A., Fundamentals of Astrodynamics and Applications, 4th ed, Microcosm Press, Hawthorne, CA, 2013.

11. ANNEX

For near circular orbits, the motion of a servicing satellite in the rotating frame of the client satellite can be expressed using the Clohessy Wiltshire [13] or Hill’s equations of motion [14]. Vallado [15] provides a closed form expression relating the position of the servicer with respect to the client satellite as

$$\begin{bmatrix} x(t) \\ y(t) \\ z(t) \\ \dot{x}(t) \\ \dot{y}(t) \\ \dot{z}(t) \end{bmatrix} = \begin{bmatrix} 4-3\cos(\omega_\oplus t) & 0 & 0 & \frac{1}{\omega_\oplus}\sin(\omega_\oplus t) & \frac{2}{\omega_\oplus}(1-\cos(\omega_\oplus t)) & 0 \\ 6\omega(\sin(\omega_\oplus t)-\omega_\oplus t) & 1 & 0 & \frac{2}{\omega_\oplus}(\cos(\omega_\oplus t)-1) & \frac{1}{\omega_\oplus}(4\sin(\omega_\oplus t)-3\omega_\oplus t) & 0 \\ 0 & 0 & \cos(\omega_\oplus t) & 0 & 0 & \frac{1}{\omega_\oplus}\sin(\omega_\oplus t) \\ 3\omega_\oplus \sin(\omega_\oplus t) & 0 & 0 & \cos(\omega_\oplus t) & 2\sin(\omega_\oplus t) & 0 \\ 6\omega_\oplus(\cos(\omega_\oplus t)-1) & 0 & 0 & -2\sin(\omega_\oplus t) & 4\cos(\omega_\oplus t)-3 & 0 \\ 0 & 0 & -\omega_\oplus \sin(\omega_\oplus t) & 0 & 0 & \cos(\omega_\oplus t) \end{bmatrix} \begin{bmatrix} x_0 \\ y_0 \\ z_0 \\ x_0 \\ y_0 \\ z_0 \end{bmatrix} \quad \text{(A1)}$$

where $\omega_\oplus$ is the mean motion of the GEO satellite which is approximately 7.29x10^{-5} radians/second and $\mathbf{x} = [x_0 \quad y_0 \quad z_0 \quad \dot{x_0} \quad \dot{y_0} \quad \dot{z_0}]^T$ is the initial state the servicer with respect to the client.